Applied Physics A (2018) 124:194
https://doi.org/10.1007/s00339-018-1629-y

Applied Physics A
Materials Science & Processing

Noble metal (Pt or Au)-doped monolayer MoS_2 as a promising adsorbent and gas-sensing material to SO_2, SOF_2 and SO_2F_2: a DFT study

Dachang Chen[1] · Xiaoxing Zhang[1,2] · Ju Tang[1] · Hao Cui[2] · Yi Li[1]

Received: 12 December 2017 / Accepted: 28 January 2018 / Published online: 31 January 2018

Abstract

We explored the adsorption of SO_2, SOF_2 and SO_2F_2 on Pt- or Au-doped MoS_2 monolayer based on density functional theory. The adsorption energy, adsorption distance, charge transfer as well as density of states were discussed. SO_2 and SOF_2 exhibit strong chemical interactions with Pt-doped MoS_2 based on large adsorption energy, charge transfer, and changes of electron orbitals in gas molecule. SO_2 also shows obvious chemisorption on Au-doped MoS_2 with apparent magnetism transfer from Au to gas molecules. The adsorption of SO_2F_2 on Pt–MoS_2 and SOF_2 on Au–MoS_2 exhibits weaker chemical interactions and SO_2F_2 losses electrons when adsorbed on Pt-MoS_2 which is different from other gas adsorption. The adsorption of SO_2F_2 on Au–MoS_2 represents no obvious chemical interaction but physisorption. The gas-sensing properties are also evaluated based on DFT results. This work could provide prospects and application value for typical noble metal-doped MoS_2 as gas-sensing materials.

1 Introduction

Nowadays, 2D materials have experienced rapid development in many field such as gas sensor, battery, catalytic materials, supercells, energy storage materials, etc. [1–3]. Layered transition metal dichalcogenides (TMDs) have unique structure and properties with widespread concern and MoS_2 monolayer is the most typical one [4]. For bulk phase of MoS_2, it has an indirect bandgap of about 1.2 eV, but the bandgap value increases as the number of layers decreases and reaches nearly 1.9 ev with conversion from indirect bandgap to direct bandgap [5]. MoS_2-based Field-Effect Transistor (FET) devices have experience a rapid development process after the first report by Radisavljevic of FET device with 1×10^8 current on/off ratio [6]. For MoS_2 and its series of modified materials, they have excellent gas sensitive properties due to their high-specific surface area, favorable adsorption properties to gas molecules.

MoS_2 monolayer used as gas-sensing materials has been first reported by Li et al. Single and multi-layers of MoS_2 were deposited on an SiO_2/Si substrate and showed high sensitivity to NO in the concentration from 0.3 to 2 ppm at room temperature [7]. MoS_2-based FET device could also be an excellent chemical gas sensor to detect triethylamine and other organics. The sensor acted as a n-type character and showed high sensitivity and selectivity to triethylamine compared with carbon nanotube [8]. The intrinsic MoS_2 devices can detect arsenite down to 0.1 ppb [9]. Moreover, the number of layers can affect the sensing properties as well. For NO_2 and NH_3 sensing, few layers of MoS_2 exhibited better sensing properties compared to monolayer and the charge transfer determined the sensitivity [10]. Not only that, MoS_2-based composite materials can promote the sensitivity and selectivity to typical gases than single component of sensing materials [11–19].

From the first-principle researches reported by several scholars, pristine MoS_2 exhibits weak interaction to most of common gases [20, 21]. To enhance the chemical interaction between typical gas molecule and MoS_2 surface, doping is one of the most effective way. The doping type includes

Electronic supplementary material The online version of this article (https://doi.org/10.1007/s00339-018-1629-y) contains supplementary material, which is available to authorized users.

✉ Xiaoxing Zhang
xiaoxing.zhang@outlook.com

1 School of Electrical Engineering, Wuhan University, Wuhan 430072, China

2 State Key Laboratory of Power Transmission Equipment and System Security and New Technology, Chongqing University, Chongqing 400044, China

metal doping and non-mental doping and metal doping is most based on transition element. The doping of N or P can enhance the performance of MoS_2 monolayer for oxygen reduction reaction to some extent [22]. In addition, transition metal doping can bring enhancement in similar realm. Zhao et al. made an elaborate discussion about the effect of doping 19 kinds of transition element on MoS_2 for ORR and the results showed that Cu-embedded MoS_2 monolayer performed the best [23]. Zhu et al. explored ten types of transition metal embedded monolayer MoS_2 to evaluate the adsorption and gas-sensing properties to five common gas molecules including adsorption energy, net charge transfer, charge density, and density of states [24]. Kadioglu et al. [25] analyzed the effect of adding Au and Cu atoms above monolayer MoS_2 to adsorb CO and H_2O molecules and found that the ratio and content of Au and Cu brought different adsorption properties. Ma et al. [26] used four different transition metal atom-doped MoS_2 monolayer, respectively, and compared the electron distribution when adsorbing CO and NO molecules. Therefore, the doping of MoS_2 monolayer makes it more active and sensitive to typical gases than pristine monolayer.

Sulfur hexafluoride(SF_6) has been used in a variety of industrial applications because of its excellent performance in insulation property. However, SF_6 will react with trace water and oxygen in gas-insulated equipment when partial discharge and local overheating appear. The relatively stable products include SO_2, SOF_2, SO_2F_2, etc. [27, 28]. The severity of these insulation defects can be obtained by means of detecting the types and concentrations of these products [29, 30]. A typical effective method is to use chemical gas sensor and a series of researches demonstrated that choosing appropriate gas-sensing materials makes it more feasibility and efficiency to detect the products [31–35].

To investigate the chemical interaction between doped MoS_2 monolayer and SF_6 decompositions to explore the prospective to become gas-sensing materials in this realm, we perform first-principle calculations toward adsorption properties of MoS_2 with typical noble metal (Pt and Au) doping. We first obtained the most energy stable adsorption structure of each gas molecule on doped surface. Then, the adsorption properties such as adsorption energy, adsorption distance, and electron transfer were calculated based on density functional theory (DFT). To further study the chemical interactions, total density of states (TDOS) and partial density of states (PDOS) before and after adsorption were discussed. The results suggest that the doping of different transition metal could be an effective method to improve the adsorption and sensing properties of MoS_2-to-SF_6 decompositions.

2 Computational methods

All the first-principles calculations were carried out using $Dmol^3$ package with density functional theory (DFT) method using linear combination of atomic orbitals (LCAO) [36, 37]. To deal with the electron exchange and correlation, Perdew–Burke–Ernzerhof function (PBE) with generalized gradient approximation (GGA) was employed [38]. We selected the double numerical plus polarization (DNP) as the atomic orbital basis set. DFT semi-core pseudopotential (DSSP) method was applied considering the relativistic effect of transition elements. It means that to reduce the quantity of calculation and increase efficiency, core electrons treatment is substituted by norm-conserving pseudopotentials. For a better description of van der Waals (VDW) interactions, the Tkatchenko and Scheffler's (TS) method was adopted [39] and we also analyzed the adsorptions without VDW interactions. For geometric optimization, we set the convergence criteria of 1.0×10^{-5}Ha, 0.002 Ha/Å, 0.005 Å for energy tolerance, maximum force, and displacement, respectively, with a smearing of 0.005Ha for accelerating convergence. For static electronic structure calculations, a more accurate 10^{-6}Ha self-consistent loop energy and a large enough global orbital cut-off radius of 5.0 Å was implemented to ensure the accurate calculation of total energy. The k-point sample of Monkhorst–Pack grid was set to $3\times3\times1$ of the Brillouin zone for geometric optimization and a more accurate k-point of $6\times6\times1$ for static energy and electronic structure calculations [40]. All the calculations were spin polarized.

We obtained an optimized lattice parameter of 3.15 Å which is in good consistence with other researches (3.14 Å, 3.16 Å for calculation) [41, 42] and experiment results (3.15 Å, 3.16 Å) [43, 44]. We built a 4×4 supercell including 16 Mo and 32 S with a vacuum region of $c=15$ Å for prevent the interaction from adjacent unit, as shown in Fig. 1. For transition metal-doped MoS_2 models, we placed one Pt or Au atom above the top site of Mo (T_{Mo}), top site of S (T_S) or hollow site (H) of the surface for geometric optimization and only the lowest energy structures were chosen for the following adsorption calculations.

We define the adsorption energy of one Pt/Au atom adsorbed on MoS_2 monolayer as the following equation:

$$E_{ad} = E_{MoS_2\text{-TM}} - E_{MoS_2\text{ monolayer}} - E_{\text{one TM atom}}, \quad (1)$$

where $E_{\text{one TM atom}}$ and $E_{MoS_2\text{ monolayer}}$ denote the total energy of one transition metal atom (Pt/Au) and optimized MoS_2 monolayer and $E_{MoS_2\text{-TM}}$ represents the total energy of one TM atom adsorbed on MoS_2 monolayer.

We also define the adsorption energy of one gas molecule adsorbed on doped MoS_2 monolayer as the following equation:

$$E_{ad} = E_{\text{molecule}/MoS_2\text{-TM}} - E_{MoS_2\text{-TM}} - E_{\text{molecule}}, \quad (2)$$

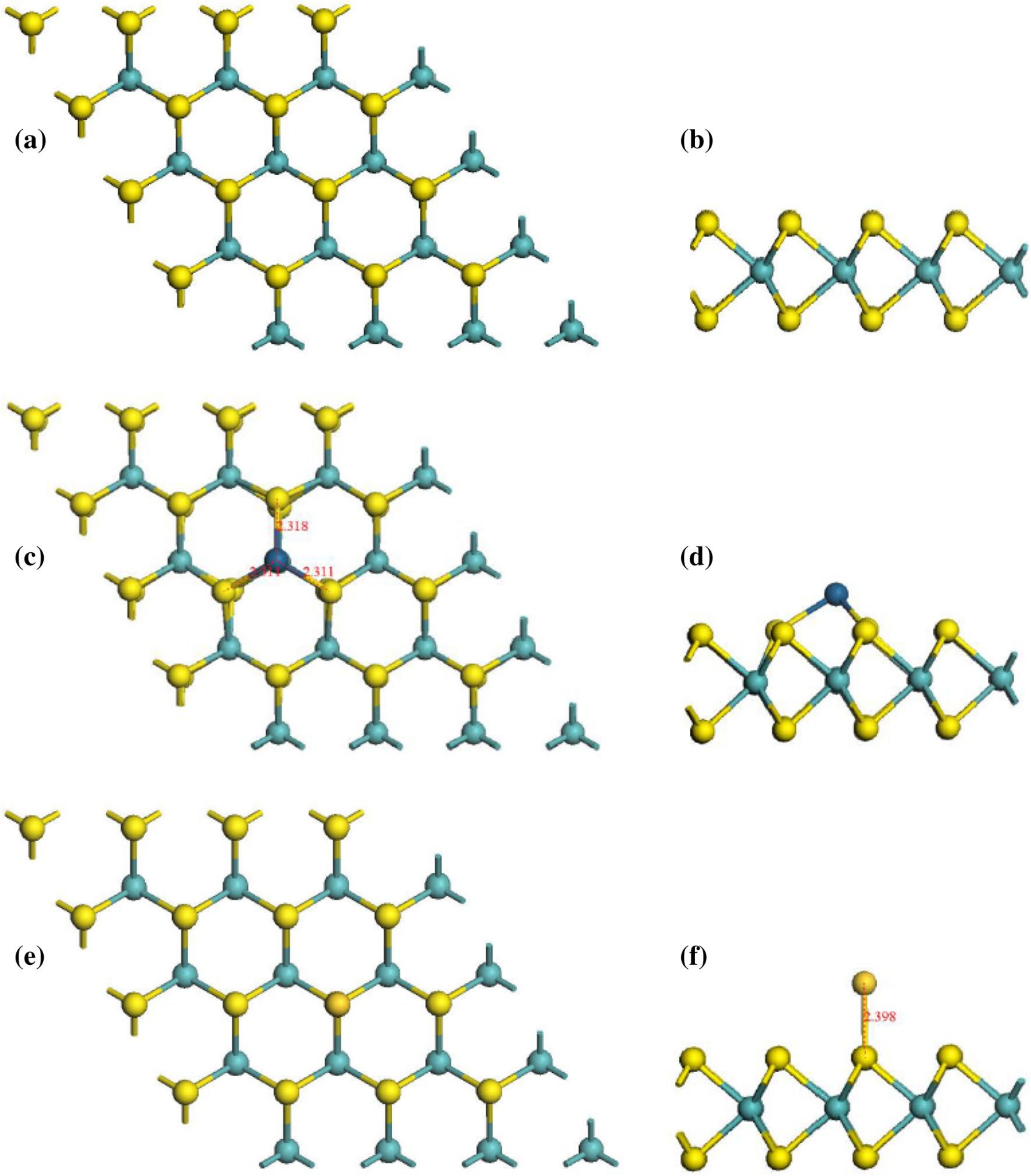

Fig. 1 Structure of MoS_2 monolayer, **a, b** pure, **c, d** decorated with Pt atom, **e, f** decorated with Au atom

where E_{molecule} and $E_{\mathrm{MoS_2\text{-}TM}}$ denote the total energy of isolated gas molecule, respectively, and optimized doped MoS_2 monolayer and $E_{\mathrm{molecule/MoS_2}}$ represents the total energy of adsorption system. We use the Hirshfeld (HI) method to define the charge transfer Q_t and a negative value means that the electrons transfer from MoS_2 to gas molecules, so the gas molecule has negative charge.

To explore the best adsorption orientation and adsorption location, we set three initial adsorption directions of SO_2 (vertical with S above, parallel, vertical with S downward), two directions of SOF_2 (S above and S downward), and two directions of SO_2F_2 (F above and O above), as shown in Fig. S1; the structure of gas molecule had been optimized using the above converge criterion and cut-off parameter and the results are shown in Table S1. All the initial distances between transition metal and S atom in molecule are set to 2.5 Å.

3 Results and discussion

3.1 Pt- and Au-doped MoS_2 monolayer

The three possible structures of one Pt/Au atom adsorbed on MoS_2 surface were tested to evaluate the most stable adsorption configuration. As shown in Fig. 1, based on the largest adsorption energy, the Pt atom is inclined to locate on the top of Mo site(T_{Mo}), while Au tends to be in top site of S(T_S). All the adsorption energies and configurations are listed in Table S2, and Figs. S1 and S2. The lengths of bonds between Pt and S are 2.31, 2.31, and 2.32 Å, and Au and S is 2.40 Å, which is strongly accords with other study [45, 46]. The TDOS are shown in Fig. 2. The Pt-doped MoS_2 structure has no magnetism with highly symmetric TDOS curve. However, due to the total magnetic moment of Au, doped MoS_2 is 1.0 μ_B; the TDOS presents a certain asymmetry especially near Fermi-level. On account of relevant, more detailed results have been reported [45, 46]; we will not discuss it furthermore. For interactions and electronic structure, we only choose the most energy favorable adsorption configuration for each gas.

3.2 SO_2 adsorption

Figure 3 shows the configuration for SO_2 adsorption on Pt- or Au-doped MoS_2 monolayer. As to Pt–MoS_2, SO_2 molecule locates nearly vertical to the surface with an adsorption distance of about 2.19 Å. The structure of SO_2 does not experience obvious change; only the angle of O–S–O has a small decrease to 119.0°. However, the distance between Pt and S on MoS_2 surface shows an increased tendency, reaching 2.39, 2.39, and 2.42 Å, respectively, while the distance between Pt and right below Mo increases from 2.80 to 2.91 Å. For SO_2 adsorbed on Au–MoS_2, the plane of molecule has an angle of about 45° with MoS_2 surface. The adsorption distance is 2.36 Å and the bond length of S–O increases to 1.48 Å with slight larger bond angle of 120.3°. Au becomes closer to S atom on surface by 2.36 Å. Considering other adsorption parameters, the adsorption of SO_2 on Pt–MoS_2 brings larger adsorption energy, but less charge transfer compared to Au–MoS_2 and SO_2 gains electrons from Pt–MoS_2 as well as Au–MoS_2.

To explore the electronic properties, we perform the TDOS and PDOS including the role of each atom orbital, as shown in Fig. 4. In Fig. 4a, the TDOS of isolated SO_2 contains six peaks in spin up and spin down, respectively, with no magnetic moment. After adsorption on Pt–MoS_2, the original highest peak near − 4 eV splits into two peaks located from − 6 to − 7 eV in DOS. The three original peaks from 0 to − 2 eV mix together to be a relatively wider peak and also the peak right to the Fermi-level becomes wider. Based on this phenomenon, the adsorption of SO_2 on Pt–MoS_2 indeed changes the electron orbitals of gas molecule. From Fig. 4d, it can be observed that the peaks of Pt and S in gas molecule near − 11, − 7, and − 6, 2 eV exhibit apparent overlap, indicating that quite strong electron orbital interaction between Pt and gas molecules. As to the adsorption on Au–MoS_2, not just the changes of peak intensity and width, the SO_2 processes a certain magnetism due to the asymmetry of navy curve, as shown in Fig. 4c. To have a further study of magnetic properties, we find that SO_2 has a magnetic moment of 0.57 μ_B after adsorption and the magnetic moment of Au decrease from 0.56 to 0.16 μ_B which demonstrates that not only charge transfer but also magnetism transfer happens when SO_2 adsorbed on Au–MoS_2. In Fig. 4e, peaks overlapping appear near − 11, − 7.5, − 6, − 2, and 0 eV. S 3s orbitals contribute more than S 3p near − 11 and − 2 eV, and for other overlap region, the case is the opposite. The relatively large adsorption energy, charge transfer, and obvious change of electron orbitals of

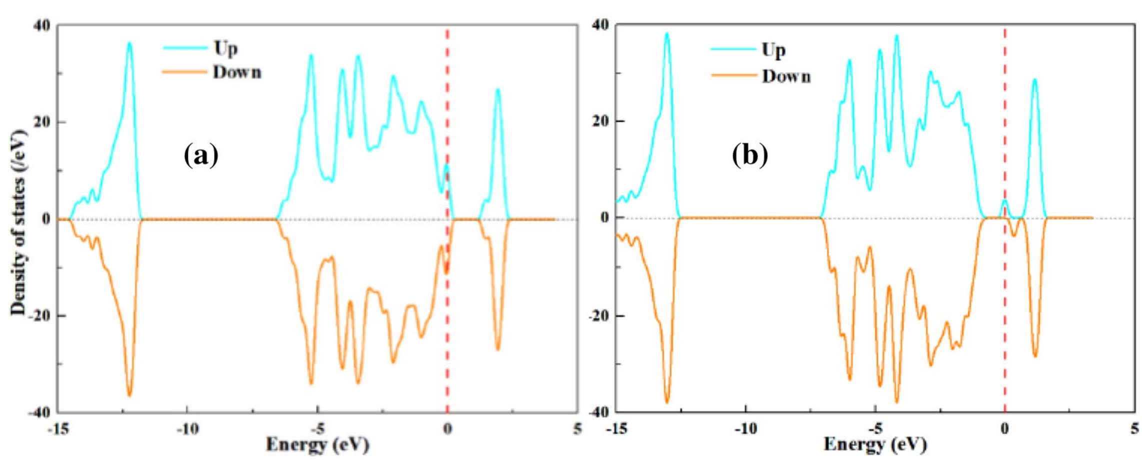

Fig. 2 DOS of **a** Pt-decorated MoS_2 monolayer, **b** Au-decorated MoS_2 monolayer

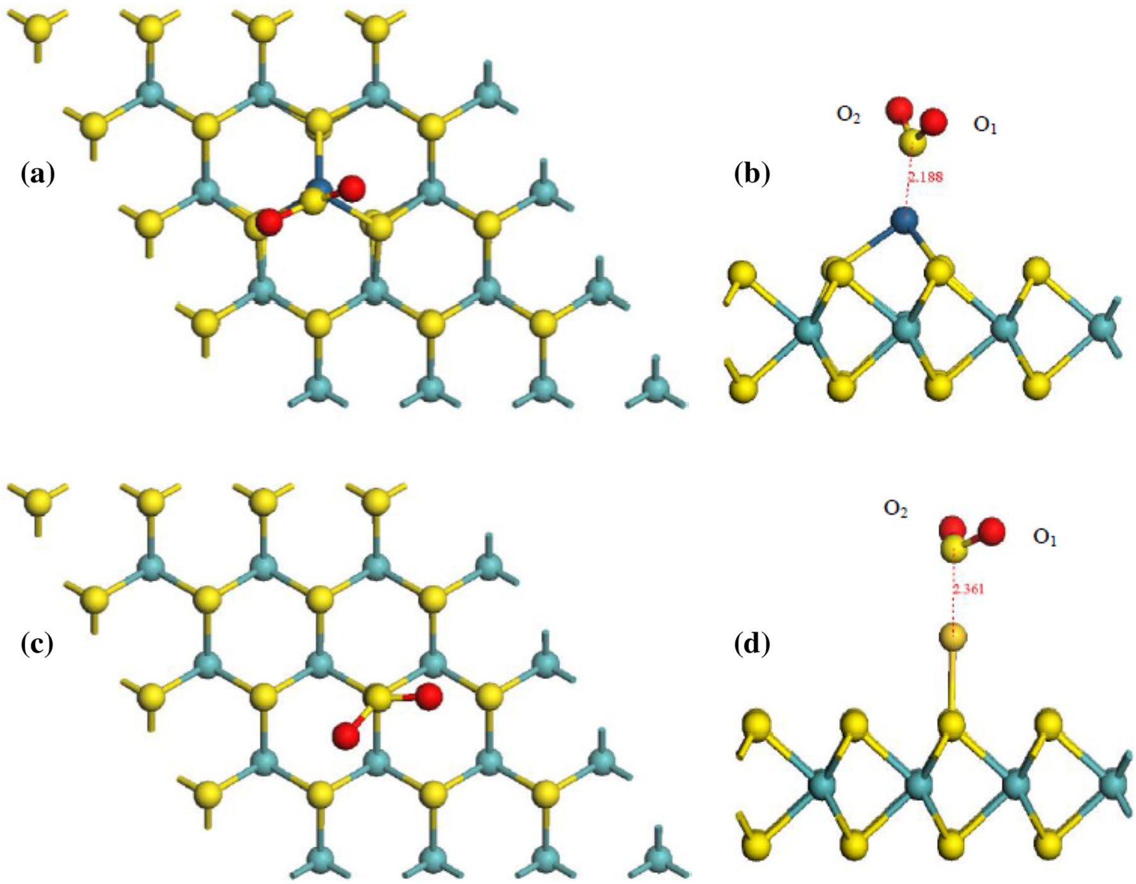

Fig. 3 Adsorption of SO_2 above **a, b** Pt-decorated MoS_2 monolayer, **c, d** Au-decorated MoS_2 monolayer

SO_2 demonstrate the obvious chemical interaction between SO_2 molecule and Pt–MoS_2 (Au–MoS_2).

3.3 SOF_2 adsorption

When SOF_2 adsorbed on doped MoS_2, the adsorption directions for Pt–MoS_2 and Au–MoS_2 are the same; that is, the S atom locates beneath other atoms in molecule. An adsorption distance of 2.19 Å for Pt–MoS_2 with no obvious change of bond lengths of gas molecule, but a little decrease of bond angles from 93.3° to 92.2° and 106.8° to 106.0°. The distances of Pt and nearest Mo increase to 2.89 Å, illustrating that Pt has the tendency of keeping away from the MoS_2 surface when SOF_2 adsorption which is similar to SO_2 adsorption. As to SOF_2 adsorbed on Au–MoS_2, the distance between Au and adjacent S on surface maintains 2.40 Å, but the bond of Au–S shows a little inclination to the surface. Moreover, dramatic variation of gas molecule appears in the elongation of S–F_2 bond which reaches 1.70 Å and changes of bond angles (105.8° to O–S–F_1 and 107.7° to O–S–F_2). The adsorption energy of SOF_2 on Pt–MoS_2 is significantly higher than Au–MoS_2 (1.370–0.332 eV), but the charge transfer between gas molecule and Au–MoS_2 is larger. We estimate that this phenomenon may be due to the partial consumed energy of translational motion of Au on surface. SOF_2 acts as an electron acceptor when adsorption on these two kinds of doped surface (Fig. 5).

For DOS analysis, the curve of isolated SOF_2 expresses several peaks with nearly the same intensity. After SOF_2 adsorbed on Pt–MoS_2, all the peaks experience left shift by about 3 eV. A new higher peak appears near − 8 eV which is mainly attributed to peak mixing near − 5 eV of isolated DOS curve and three peaks near − 5 eV of adsorbed SOF_2 can be ascribed to peak mixing from − 3 to − 1 eV in isolated SOF_2. As it can be seen, the electron orbitals of SOF_2 experience certain changes when it adsorbed on Pt–MoS_2. In Fig. 6d, the Pt 5d orbitals overlap with S 3 s near − 13 eV, with S 3p near − 13, − 8.5, − 7, − 5, and − 3 eV and the Pt 6p orbitals overlap with S 3p near − 0.5 eV. These overlaps indicate the orbital interaction between Pt and gas molecules. As to gas molecule adsorbed on Au–MoS_2, the peaks near − 5 eV of adsorbed SOF_2 experience peak mixing compared with isolated SOF_2 near − 2 eV. In addition, the DOS curve of adsorbed molecule shows slight asymmetry indicating the non-zero magnetic moment of adsorbed SOF_2. The calculated magnetic moment of adsorbed SOF_2 is 0.31

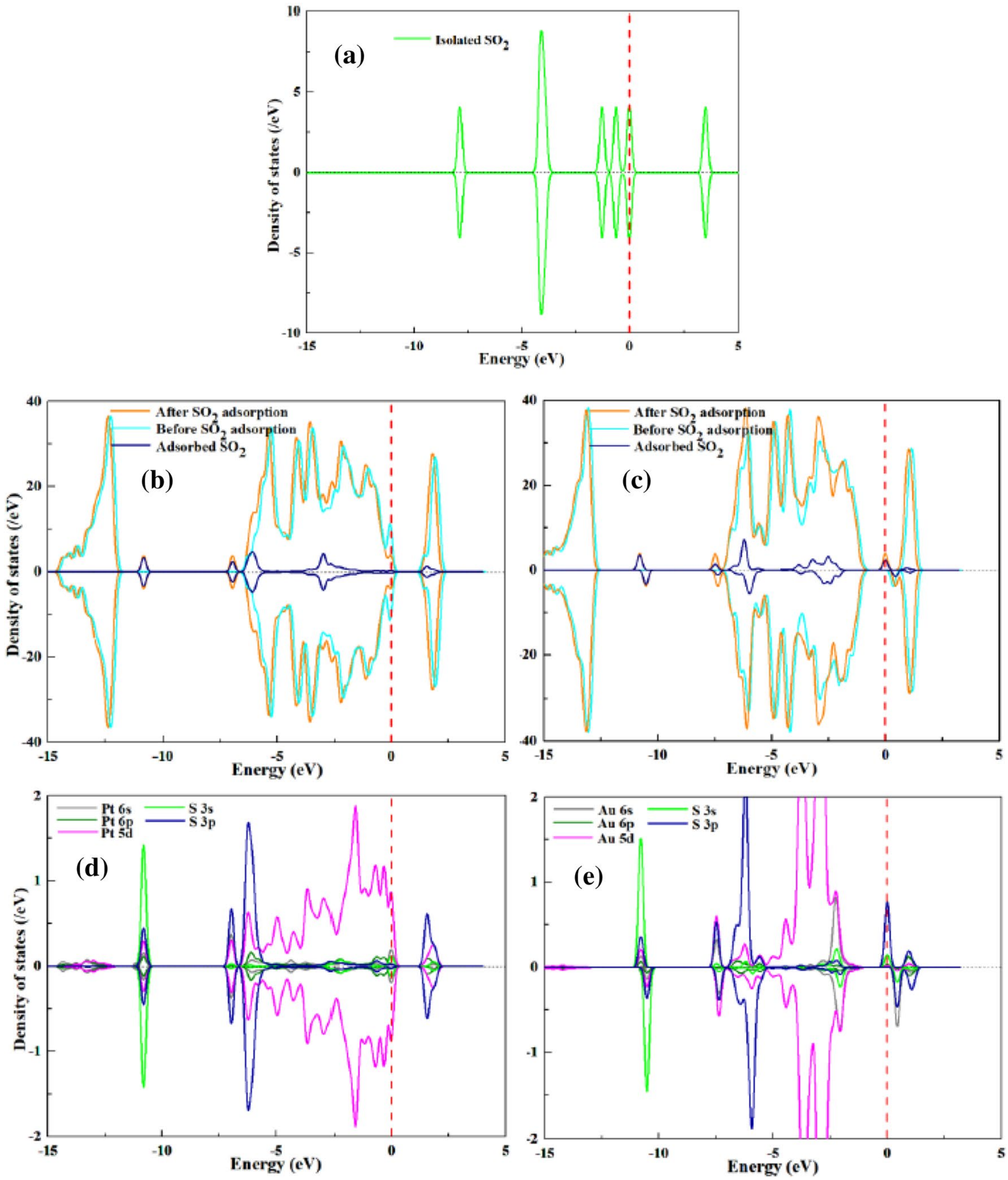

Fig. 4 **a** TDOS of SO_2, **b, d** TDOS and PDOS of SO_2 adsorbed on Pt-decorated MoS_2 monolayer, **c, e** TDOS and PDOS of SO_2 adsorbed on Au-decorated MoS_2 monolayer

μ_B which is lower than adsorbed SO_2 and a decline of magnetic moment to 0.26 μ_B for Au atom also indicates partial magnetic transfer from Au–MoS_2 to SOF_2. In Fig. 6e, Au 5d orbitals overlap with S 3s near − 8.5 eV and S 3p near − 8.5 and − 5 eV, while Au 6s orbitals overlap with S 3s and S 3p near 0 eV. Based on the DOS changes of molecule before and after adsorption and overlap in electron orbital, there exists some chemical interactions between Au–MoS_2 and SOF_2, but these interactions are weaker compared with SO_2 adsorption on Au–MoS_2 due to the less adsorption energy, charge transfer, magnetism transfer and orbital overlaps.

3.4 SO_2F_2 adsorption

For SO_2F_2 adsorbed on Pt–MoS_2, the distance between Pt and adjacent Mo is 2.78 Å with little change compared to

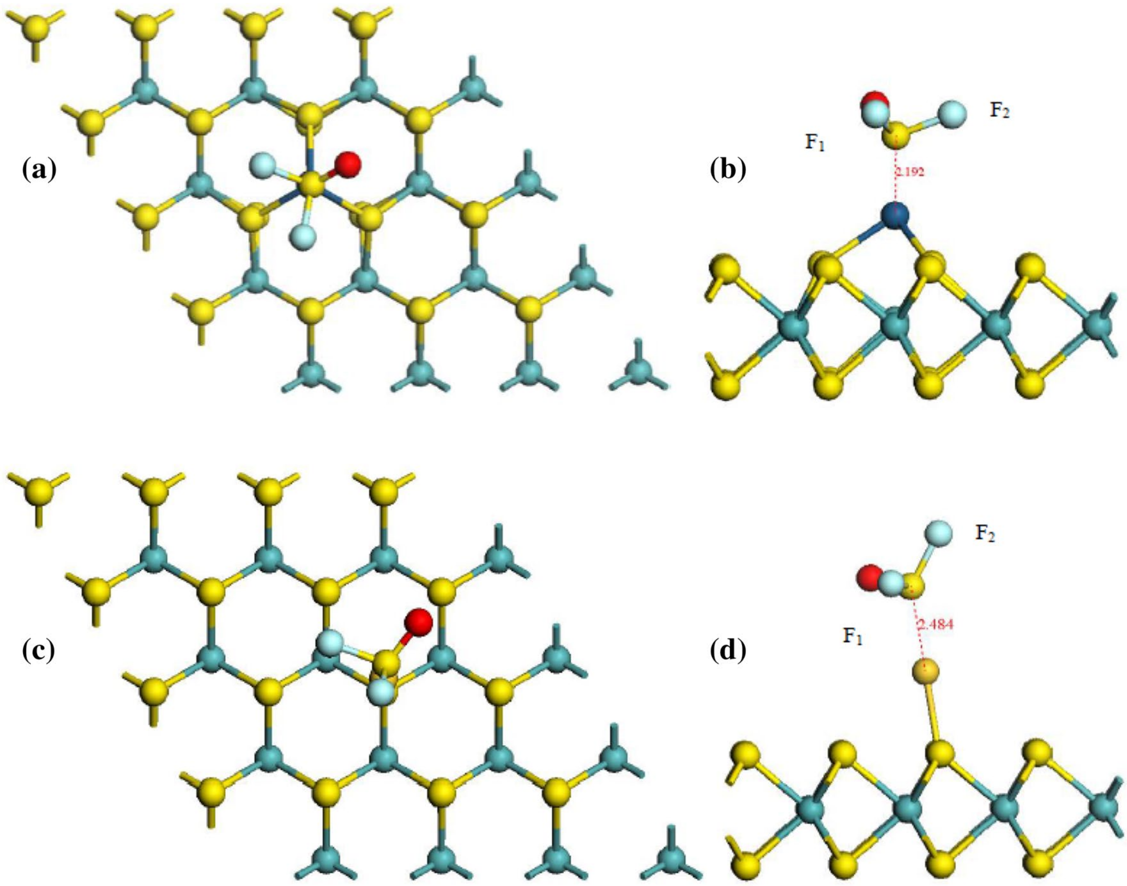

Fig. 5 Adsorption of SOF_2 above **a, b** Pt-decorated MoS_2 monolayer, **c, d** Au-decorated MoS_2 monolayer

the initial distance of 2.79 Å and the structure of gas molecule remains nearly unchanged except the little increase of S–O_1 by 0.02 Å. When SO_2F_2 adsorbed on Au–MoS_2, it shows a very large adsorption distance of 3.32 Å with small adsorption energy of 0.175 eV, and the structure of MoS_2 also remains unchanged with only little transitional movement of Au (Fig. 7).

To ensure whether electron orbital interaction appears between SO_2F_2 and doped MoS_2, DOS was discussed in detail. TDOS of SO_2F_2 shows a symmetrical curve of several peaks with the same intensity and one higher peak near −2.7 eV. After SO_2F_2 adsorbed on Pt-MoS_2, we notice that two initial peaks near Fermi-level coalesce into one peak with larger intensity located near −4.5 eV in DOS of adsorbed SO_2F_2 and beyond that the intensity and relative position of other initial peaks do not show a clear change. For PDOS of every orbital, it can only be seen that slight overlap between Pt 6 s and O_1 2p near −6.5 eV, Pt 5d and O_1 2p near −4.5 eV where peak mixing happens in gas molecule. As to gas adsorbed on Au–MoS_2, one can see that all the peaks of gas molecule have evidently not changed including intensity and relative position, only left shift by about 4 eV. It should be noted that the left shift is only due to the different Fermi levels of isolated SO_2F_2 and Au–MoS_2, so only the left shift could not indicate the change of electron orbitals in gas molecule. Despite of this, the high symmetry of navy curve in Fig. 8c illustrates no magnetic moment change after adsorption. As a result, the structure as well as the electron orbitals of gas molecule shows no obvious variation after adsorbed on Au–MoS_2. The phenomenon indicates that only physical interaction rather than chemical adsorption appears between SO_2F_2 and Au–MoS_2.

3.5 Summarizing of adsorption properties and forecasting of sensing application

All the parameters of SO_2, SOF_2, and SO_2F_2 adsorbed on Pt–MoS_2 and Au–MoS_2 are listed in Table 1 and Table S4. All the adsorption energies experience a certain degree of reduction when not adopting TS method, but the values of charge transfer and adsorption distance do not change much. The interaction between SO_2F_2 and Au–MoS_2 is mainly VDW force, and for different adsorptions, the proportion of VDW force is different. To consider the negligible

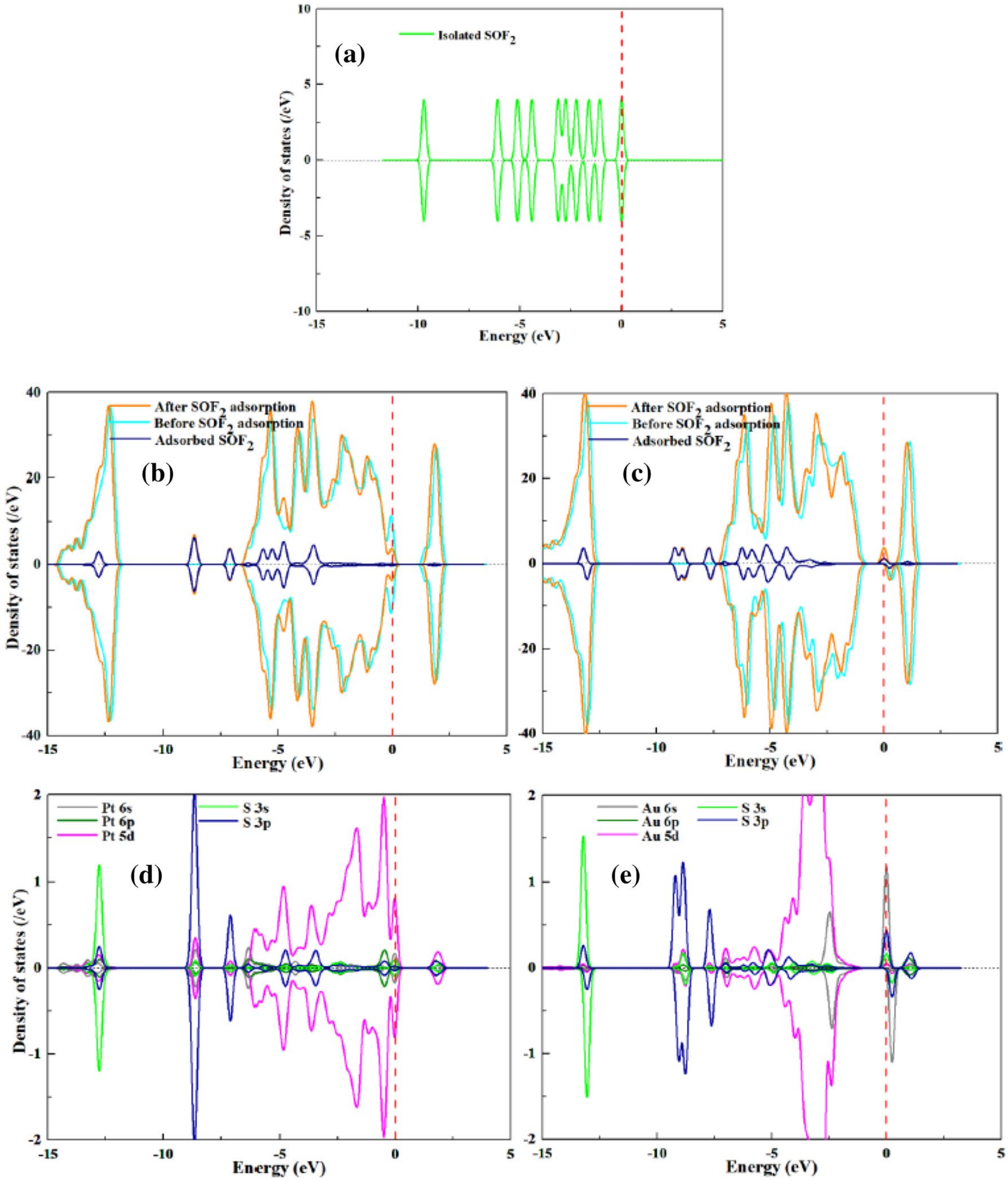

Fig. 6 **a** TDOS of SOF_2, **b, d** TDOS and PDOS of SOF_2 adsorbed on Pt-decorated MoS_2 monolayer, **c, e** TDOS and PDOS of SO_2 adsorbed on Au-decorated MoS_2 monolayer

role of VDW interactions, we mainly focus on the results obtained using TS method. Due to the negative value of adsorption energies, all the adsorptions are exothermic process. For a gas sensor, the sensitivity depends on both the adsorption energy and charge transfer [10]. The adsorption energy of Pt–MoS_2 shows generally greater than Au–MoS_2. Larger adsorption energy could bring greater adsorption amount and interaction between gases and adsorbent. For SO_2 and SOF_2 adsorption on Pt–MoS_2, the adsorption distance (2.19 Å) is even smaller than the sum of single-bond covalent radii of Pt and S (2.26 Å) which can also indicate the strong chemical interaction between Pt–MoS_2 and SO_2, SOF_2, and even new chemical bond formation [47]. As to SO_2F_2 adsorbed on Au-MoS_2, the distance between Au and O_1 is 3.32 Å; much larger than 1.87 Å (the sum of covalent radii of Au and O) can also prove the weak interaction

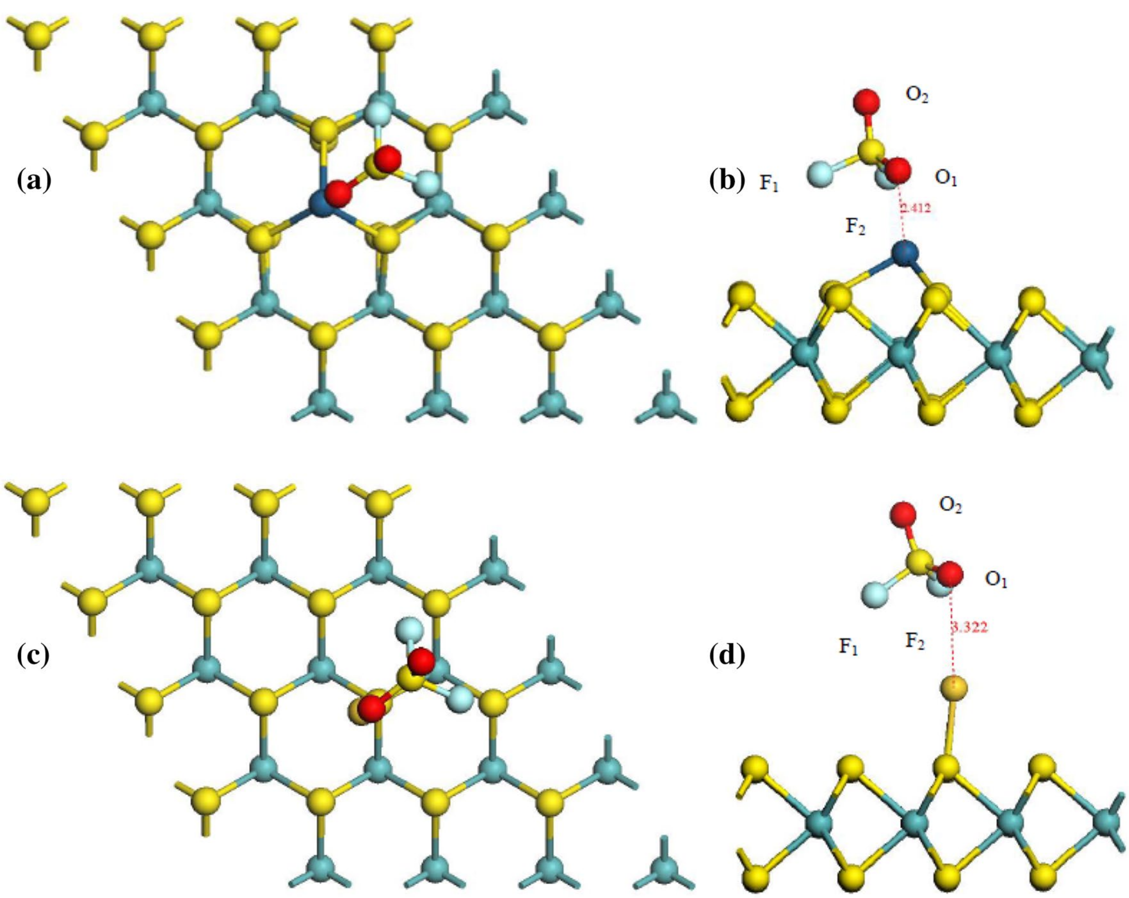

Fig. 7 Adsorption of SO_2F_2 above **a, b** Pt-decorated MoS_2 monolayer, **c, d** Au-decorated MoS_2 monolayer

between them. The adsorption energy of SO_2 on Au–MoS_2 is also quite large (− 0.946 eV) with the greatest charge transfer, reaching 0.222e. Charge transfer is one of the most important parameter affecting sensitivity [10]. More charge transfer with the same adsorption amount can give rise to larger sensitivity. For SO_2F_2 adsorbed on Pt-MoS_2, the direction of charge transfer is the opposite compared with other gases which can cause the resistance change of sensor in the opposite direction. Another important parameter of a gas sensor is the recovery properties. Although larger adsorption energy and charge transfer bring greater sensitivity, the sensitivity is at the price of recovery property. If strong chemical interaction happens between gases and surface, it is difficult for desorption resulting in long recovery time. Based on the transition state theory and Van't–Hoff–Arrhenius expression [48], the recovery time could be defined as:

$$\tau = A^{-1}\mathrm{e}^{(-E_\mathrm{a}/RT)}, \tag{3}$$

where A, R, and T represent the apparent frequency factor, Boltzmann's constant, and temperature, respectively, and E_a refers to the activation energy. For desorption process, the activation energy can be seen as the above adsorption energy E_ad. If the factor A does not change much with different types of gases and different metal doping, the smaller adsorption energy could bring the shorter recovery time at the same temperature. Comparing the adsorption energy of gas molecule on Pt–MoS_2 and Au–MoS_2, SO_2, and SOF_2 is very difficult to desorb from Pt–MoS_2 unless elevating the working temperature. Due to the better desorption property of Au–MoS_2 than Pt-MoS_2, the working temperature of Au–MoS_2 can be lower than Pt–MoS_2. In short, both Pt–MoS_2 and Au–MoS_2 will have high sensitivity to SO_2, but Au–MoS_2 has a better recovery property so it can work at a lower temperature than Pt–MoS_2. For SOF_2 sensor, the sensitivity of Pt–MoS_2 will be much higher than Au–MoS_2, so Pt–MoS_2 is more suitable for SOF_2 sensing, but the working temperature should be relatively high to guarantee the shorter recovery time. As to SO_2F_2 sensor, Pt–MoS_2 may experiences a different direction of resistance change compared to SO_2 and SOF_2, and the recovery property is also better because of the very weak interaction between Au–MoS_2 and SO_2F_2, Au–MoS_2 is not suitable for SO_2F_2 sensing due to the low sensitivity.

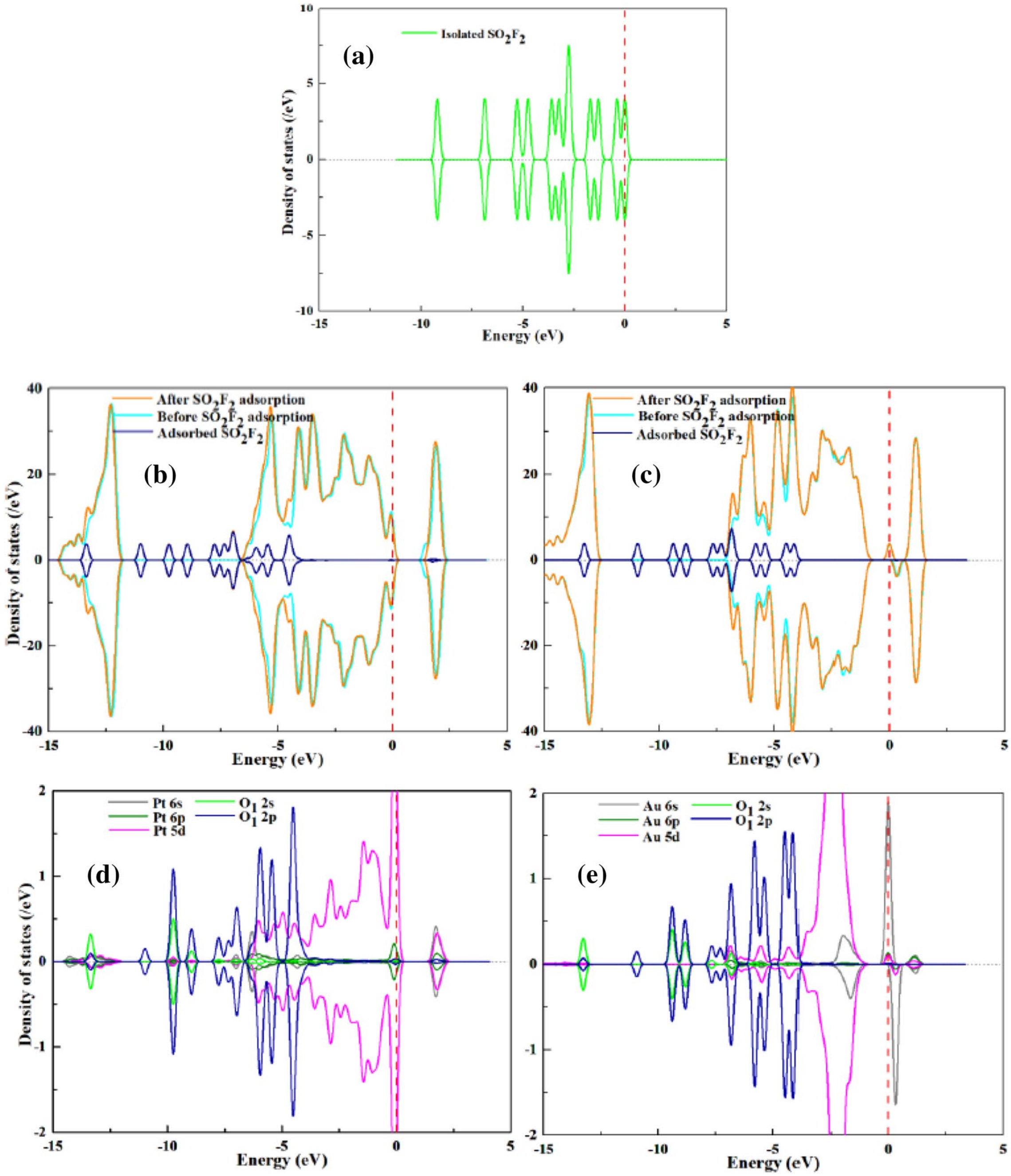

Fig. 8 **a** TDOS of SO_2F_2, **b, d** TDOS and PDOS of SOF_2 adsorbed on Pt-decorated MoS_2 monolayer, **c, e** TDOS and PDOS of SO_2 adsorbed on Au-decorated MoS_2 monolayer

4 Conclusions

To explore the adsorption behavior and estimate the gas-sensing properties of Pt- and Au-doped MoS_2 monolayer, density functional theory was used to calculate the adsorption energy, charge transfer, adsorption distance, and density of states. For SO_2, both Pt–MoS_2 and Au–MoS_2 exhibit relatively large adsorption energy and charge transfer with strong chemical interactions due to the obvious change of electron orbitals in gas molecule and orbital interactions between Au on surface and S in molecule. More than that, SO_2 adsorption will introduce magnetism transfer from Au–MoS_2 to molecule to some extent. For SOF_2, the adsorption energy of Pt–MoS_2 is much greater than that of Au–MoS_2, but the charge transfer comparison is the opposite. The adsorption of SOF_2 also brings different levels of changing in electron orbitals of gas molecule on both Pt–MoS_2 and Au–MoS_2 and magnetism transfer on Au–MoS_2. As to SO_2F_2, the

Table 1 Adsorption energy (E_{ad}), adsorption distances (D) and charge transfer (Q_t) of structures of SO_2, SOF_2, and SO_2F_2 adsorption on Pt/Au-decorated MoS_2

Structure	E_{ads} (eV)	Q_t (e)	D (Å)
Pt-MoS_2/SO_2	−1.543	−0.109	2.19 (Pt–S)
Pt-MoS_2/SOF_2	−1.370	−0.066	2.19 (Pt–S)
Pt-MoS_2/SO_2F_2	−0.453	0.116	2.41 (Pt–O_1)
Au-MoS_2/SO_2	−0.946	−0.222	2.36 (Au–S)
Au-MoS_2/SOF_2	−0.332	−0.095	2.48 (Au–S)
Au-MoS_2/SO_2F_2	−0.175	0.002	3.32 (Au–O_1)

interactions between gas molecule and surface are weaker than the above two gases. The SO_2F_2 acts as an electron donor when adsorbed on Pt–MoS_2 which is different from other gases. No chemical interactions are found when SO_2F_2 adsorbed on Au–MoS_2 for the reason that electron orbitals of gas molecule remain constant with little orbital interactions between Au and SO_2F_2. Moreover, the application possibility of Pt–MoS_2 and Au–MoS_2 using as gas-sensing material to detect these three types of gases was estimated using the conventional transition state theory. This study could provide fundamental basis for typical noble metal-doped MoS_2 as gas-sensing material to detect typical decompositions of sulfur hexafluoride in gas-insulated equipment for achieving industrial application.

Acknowledgements We gratefully acknowledge the financial support from the National Natural Science Foundation of P. R. China (Project No. 51777144) and National High-tech R&D Program of China (Project No. 2015AA050204).

References

1. C. Tan, X. Cao, X.J. Wu, Q. He, J. Yang, X. Zhang et al., Recent advances in ultrathin two-dimensional nanomaterials. Chem. Rev. **117**(9), 6225–6331 (2017)
2. M. Xu, T. Liang, M. Shi, H. Chen, Graphene-like two-dimensional materials. Chem. Rev. **113**(5), 3766–3798 (2013)
3. Q. Fu, X. Bao, Surface chemistry and catalysis confined under two-dimensional materials. Chem. Soc. Rev. **46**(7), 1842–1874 (2017)
4. M. Chhowalla, H.S. Shin, G. Eda, L.J. Li, K.P. Loh, H. Zhang, The chemistry of two-dimensional layered transition metal dichalcogenide nanosheets. Nat. Chem. **5**(4), 263–275 (2013)
5. K.F. Mak, C. Lee, J. Hone, J. Shan, T.F. Heinz, Atomically thin MoS_2: a new direct-gap semiconductor. Phys. Rev. Lett. **105**(13), 136805 (2010)
6. B. Radisavljevic, A. Radenovic, J. Brivio, I.V. Giacometti, A. Kis, Single-layer MoS_2 transistors. Nat. Nanotechnol. **6**(3), 147–150 (2011)
7. H. Li, Z. Yin, Q. He, H. Li, X. Huang, G. Lu et al., Fabrication of single and multilayer MoS_2 film based field effect transistors for sensing NO at room temperature. Small. **8**(1), 63–67 (2012)
8. F.K. Perkins, A.L. Friedman, E. Cobas, P.M. Campbell, G.G. Jernigan, B.T. Jonker, Chemical vapor sensing with monolayer MoS_2. Nano Lett. **13**(2), 668–673 (2013)
9. P. Li, D. Zhang, Y.E. Sun, H. Chang, J. Liu, N. Yin, Towards intrinsic MoS_2 devices for high performance arsenite sensing. Appl. Phys. Lett. **109**(6), 063110 (2016)
10. D.J. Late, Y.K. Huang, B. Liu, J. Acharya, S.N. Shirodkar, J. Luo et al., Sensing behavior of atomically thin-layered MoS_2 transistors. Acs Nano. **7**(6), 4879–4891 (2013)
11. D. Sarkar, X. Xie, J. Kang, H. Zhang, W. Liu, J. Navarrete et al., Functionalization of transition metal dichalcogenides with metallic nanoparticles: implications for doping and gas-sensing. Nano Lett. **15**(5), 2852–2862 (2015)
12. Y. Niu, R. Wang, W. Jiao, G. Ding, L. Hao, F. Yang, X. He, MoS_2 graphene fiber based gas sensing devices. Carbon **95**, 34–41 (2015)
13. H. Yan, P. Song, S. Zhang, J. Zhang, Z. Yang, Q. Wang, A low temperature gas sensor based on Au-loaded MoS_2 hierarchical nanostructures for detecting ammonia. Ceram. Int. **42**(7), 9327–9331 (2016)
14. N. Yue, J. Weicheng, W. Rongguo, D. Guomin, H. Yifan, Hybrid nanostructures combining graphene–MoS_2 quantum dots for gas sensing. J. Mater. Chem. A **4**(21), 8198–8203 (2016)
15. D.H. Baek, J. Kim, MoS_2 gas sensor functionalized by Pd for the detection of hydrogen. Sensors Actuators B Chem. **250**, 686–691 (2017)
16. D. Zhang, J. Wu, P. Li, Y. Cao, Room-temperature SO_2 gas-sensing properties based on a metal-doped MoS_2 nanoflower: an experimental and density functional theory investigation. J. Mater. Chem. A **5**(39), 20666–20677 (2017)
17. D. Zhang, Y.E. Sun, P. Li, Y. Zhang, Facile fabrication of MoS_2-modified SnO_2 hybrid nanocomposite for ultrasensitive humidity sensing. ACS Appl. Mater. Interfaces **8**(22), 14142–14149 (2016)
18. D. Zhang, C. Jiang, P. Li, Y.E. Sun, Layer-by-layer self-assembly of Co_3O_4 nanorod-decorated MoS_2 nanosheet-based nanocomposite toward high-performance ammonia detection. ACS Appl. Mater. Interfaces **9**(7), 6462–6471 (2017)
19. D. Zhang, Z. Wu, P. Li, X. Zong, G. Dong, Y. Zhang, Facile fabrication of polyaniline/multi-walled carbon nanotubes/molybdenum disulfide ternary nanocomposite and its high-performance ammonia-sensing at room temperature. Sensors Actuators B Chem. **258**, 895–905 (2018)
20. S. Zhao, J. Xue, W. Kang, Gas adsorption on MoS_2 monolayer from first-principles calculations. Chem. Phys. Lett. **595**, 35–42 (2014)
21. A. Shokri, N. Salami, Gas sensor based on MoS_2 monolayer. Sensors Actuators B Chem. **236**, 378–385 (2016)
22. H. Zhang, Y. Tian, J. Zhao, Q. Cai, Z. Chen, Small dopants make big differences: enhanced electrocatalytic performance of MoS_2 monolayer for oxygen reduction reaction (ORR) by N- and P-doping. Electrochim. Acta **225**, 543–550 (2017)
23. Z. Wang, J. Zhao, Q. Cai, F. Li, Computational screening for high-activity MoS_2 monolayer-based catalysts for the oxygen reduction reaction via substitutional doping with transition metal. J. Mater. Chem. A **5**(20), 9842–9851 (2017)
24. Y. Fan, J. Zhang, Y. Qiu, J. Zhu, Y. Zhang, G. Hu, A DFT study of transition metal (Fe, Co, Ni, Cu, Ag, Au, Rh, Pd, Pt and Ir)-embedded monolayer MoS_2 for gas adsorption. Comput. Mater. Sci. **138**, 255–266 (2017)
25. Y. Kadioglu, G. Gökoğlu, O. Aktürk, Molecular adsorption properties of CO and H2O on Au-, Cu-, and AuxCuy-doped MoS_2 monolayer. Appl. Surf. Sci. **425**, 246–253 (2017)
26. D. Ma, W. Ju, T. Li, X. Zhang, C. He, B. Ma et al., The adsorption of CO and NO on the MoS_2 monolayer doped with Au, Pt, Pd, or Ni: A first-principles study. Appl. Surf. Sci. **383**, 98–105 (2016)

27. F.Y. Chu, SF6 decomposition in gas-insulated equipment. IEEE Trans. Electr. Insul. (5), 693–725 (1986)
28. J. Tang, F. Liu, X. Zhang, Q. Meng, J. Zhou, Partial discharge recognition through an analysis of SF6 decomposition products part 1: decomposition characteristics of SF6 under four different partial discharges. IEEE Trans. Dielectr. Electr. Insul. **19**(1), 29–36 (2012)
29. J. Tang, F. Liu, Q. Meng, X. Zhang, J. Tao, Partial discharge recognition through an analysis of SF6 decomposition products part 2: feature extraction and decision tree-based pattern recognition. IEEE Trans. Dielectr. Electr. Insul. **19**(1), 37–44 (2012)
30. S. Li, J. Li, Condition monitoring and diagnosis of power equipment: review and prospective. High Volt. **2**(2), 82–91 (2017)
31. J. Suehiro, G. Zhou, M. Hara, Detection of partial discharge in SF6 gas using a carbon nanotube-based gas sensor. Sensors Actuators B Chem. **105**(2), 164–169 (2005)
32. H. Dai, P. Xiao, Q. Lou, Application of SnO2/MWCNTs nanocomposite for SF6 decomposition gas sensor. Phys. Status Solidi **208**(7), 1714–1717 (2011)
33. X. Zhang, J. Zhang, Y. Jia, P. Xiao, J. Tang, TiO2 nanotube array sensor for detecting the SF6 decomposition product SO2. Sensors **12**(3), 3302–3313 (2012)
34. S. Peng, G. Wu, W. Song, Q. Wang, Application of flower-like ZnO nanorods gas sensor detecting SF6 decomposition products. J. Nanomater. **2013**, 1 (2013)
35. X. Zhang, L. Yu, X. Wu, W. Hu, Experimental sensing and density functional theory study of H2S and SOF2 adsorption on Au-modified graphene. Adv. Sci. **2**(11), (2015)
36. B. Delley, An all-electron numerical method for solving the local density functional for polyatomic molecules. J. Chem. Phys. **92**(1), 508–517 (1990)
37. B. Delley, From molecules to solids with the DMol3 approach. J. Chem. Phys. **113**(18), 7756–7764 (2000)
38. J.P. Perdew, K. Burke, M. Ernzerhof, Generalized gradient approximation made simple. Phys. Rev. Lett. **77**(18), 3865 (1996)
39. A. Tkatchenko, R.A. DiStasio Jr, M. Head-Gordon, M. Scheffler, Dispersion-corrected Møller–Plesset second-order perturbation theory. J. Chem. Phys. **131**(9), 094106 (2009)
40. H.J. Monkhorst, J.D. Pack, Special points for Brillouin-zone integrations. Phys. Rev. B **13**(12), 5188 (1976)
41. L. Gao, Z.D. Yang, G. Zhang, A theoretical study for electronic and transport properties of covalent functionalized MoS_2 monolayer. Chem. Phys. 490, 29–37 (2017)
42. R. Kronberg, M. Hakala, N. Holmberg, K. Laasonen, Hydrogen adsorption on MoS_2-surfaces: A DFT study on preferential sites and the effect of sulfur and hydrogen coverage. Phys. Chem. Chem. Phys. **19**, 16231–16241 (2017)
43. R.G. Dickinson, L. Pauling, The crystal structure of molybdenite. J. Am. Chem. Soc. **45**(6), 1466–1471 (1923)
44. D. Yang, S.J. Sandoval, W.M.R. Divigalpitiya, J.C. Irwin, R.F. Frindt, Structure of single-molecular-layer MoS_2. Phys. Rev. B **43**(14), 12053 (1991)
45. P. Wu, N. Yin, P. Li, W. Cheng, M. Huang, The adsorption and diffusion behavior of noble metal adatoms (Pd, Pt, Cu, Ag and Au) on a MoS_2 monolayer: a first-principles study. Phys. Chem. Chem. Phys. **19**(31), 20713–20722 (2017)
46. J. Chang, S. Larentis, E. Tutuc, L.F. Register, S.K. Banerjee, Atomistic simulation of the electronic states of adatoms in monolayer MoS_2. Appl. Phys. Lett. **104**(14), 141603 (2014)
47. P. Pyykkö, M. Atsumi, Molecular single-bond covalent radii for elements 1–118. Chem. A Eur. J. **15**(1), 186–197 (2009)
48. Y.H. Zhang, Y.B. Chen, K.G. Zhou, C.H. Liu, J. Zeng, H.L. Zhang, Y. Peng, Improving gas sensing properties of graphene by introducing dopants and defects: a first-principles study. Nanotechnology. **20**(18), 185504 (2009)